Near-Optimal Near-Field Beam Training: From Searching to Inference

Zhuo Xu, *Graduate Student Member, IEEE*, Zijian Zhang, *Graduate Student Member, IEEE*, and Linglong Dai, *Fellow, IEEE*

***Abstract*—In extremely large-scale multiple input multiple output (XL-MIMO) systems, near-field beam training (NFBT) is an essential way to acquire channel state information (CSI) knowledge. To reduce the high training overhead caused by the distance dimension of the near-field codebook, some overhead-reduced NFBT schemes were proposed in the literature. However, existing schemes ignore the correlation between different near-field beams, which promises to provide prior knowledge for the reduction of training overhead. Aligned with this vision, this paper proposes a Bayesian regression (BAR)-based NFBT scheme, which fully utilizes the strong correlation between near-field codewords to achieve near-optimal and low-overhead NFBT. Specifically, inspired by Bayesian regression, we model the received signal corresponding to different codewords as a Gaussian process. Then, the optimal codeword can be determined by iteratively updating the posterior distribution and designing the codeword searching order. Besides, different codeword inference strategies are analyzed and compared. The proposed scheme only requires searching for a few codewords instead of the entire codebook thus avoiding the high training overhead. Simulation results verify that, compared to the existing schemes, the proposed scheme can significantly reduce the training overhead while maintaining a near-optimal achievable rate performance.**

***Index Terms*—Beam training, Bayesian regression, near-field, extremely large-scale MIMO (XL-MIMO).**

I. Introduction

TO EMPOWER burgeoning applications such as digital replica, the six-generation (6G) communication is presumed to improve 10-fold spectrum efficiency compared to 5G [1]. To achieve this vision, extremely large-scale MIMO (XL-MIMO) is proposed as one of the potential key technologies in 6G [2]. Different from massive MIMO systems in 5G, XL-MIMO deploys extremely large-scale antenna arrays (ELAA), which could achieve high spatial resolution and spatial multiplexing gain [3], [4], [5]. To fully utilize the high diversity-multiplexing gains provided by XL-MIMO, obtaining precise channel state information (CSI) is especially crucial and beam training is an efficient way to acquire CSI. Specifically, the process of beam training is carried out through searching codewords which correspond to beamforming vectors from a predefined codebook and determining the optimal codeword that maximizes the achievable rate of MIMO systems.

A. Prior Works

Generally, the electromagnetic radiation field could be broadly classified into three categories: Reactive near-field, radiative near-field, and far-field region [6]. As the reactive near-field region is negligible in practical wireless systems, for illustration simplicity, "near-field" in this paper particularly refers to "radiative near-field". In 5G massive MIMO systems, as the array aperture of the base station (BS) is not large and the near-field region is limited, the far-field channel can be modeled by planar-wave presentations, which can be fully characterized by Fourier orthogonal bases. Therefore, the discrete Fourier transform (DFT) codebook is widely used for the far-field beam training (FFBT), where each codeword corresponds to a far-field beam focusing on specific spatial angle like a flashlight [7].

In contrast, with the increasing number of antennas in XL-MIMO systems, the near-field region is enlarged and it should be accurately modeled by the spherical-wave model. Unlike the far-field channel only related to the angle, the near-field channel is determined by both angle and distance. Accordingly, the near-field polar-domain codebook is proposed in [8]. Specifically, it divides the entire space into different "angle-distance" grids, where the angle is uniformly sampled and the distance is non-uniformly sampled. Therefore, each polar-domain codeword corresponds to a beamforming vector, which could focus the beam on specific locations like a spotlight [9]. Compared to the DFT codebook, the polar-domain codebook considers an additional distance dimension, whose size is the product of the number of angle and distance sampling grids. As a result, if the exhaustive searching of the polar-domain codebook is carried out, it will face the challenge of high training overhead.

To reduce the high overhead of XL-MIMO beam training, several low-overhead near-field beam training (NFBT)

Received 8 November 2024; revised 4 March 2025 and 27 April 2025; accepted 10 May 2025. Date of publication 28 May 2025; date of current version 14 November 2025. This work was supported in part by the National Science Fund for Distinguished Young Scholars under Grant 62325106, in part by the National Key Research and Development Program of China under Grant 2023YFB3811503, and in part by the National Natural Science Foundation of China under Grant 62031019. The associate editor coordinating the review of this article and approving it for publication was B. Shim. *(Corresponding author: Linglong Dai.)*

Zhuo Xu and Zijian Zhang are with the Department of Electronic Engineering and the State Key Laboratory of Space Network and Communications, Tsinghua University, Beijing 100084, China (e-mail: xz23@mails.tsinghua.edu.cn; zhangzj20@mails.tsinghua.edu.cn).

Linglong Dai is with the Department of Electronic Engineering and the State Key Laboratory of Space Network and Communications, Tsinghua University, Beijing 100084, China, and also with the Department of Electrical Engineering and Computer Science, Massachusetts Institute of Technology, Cambridge, MA 02139 USA (e-mail: daill@tsinghua.edu.cn).

Digital Object Identifier 10.1109/TWC.2025.3571488

schemes have been proposed. Among these schemes, there are two typical representative categories: two-phase scheme and hierarchical scheme. For the first category, the two-phase NFBT scheme was proposed in [10], where in the first phase the angle is searched and selected through the DFT codebook and the distance is determined in the second phase. Furthermore, a joint angle and range estimation scheme was proposed in [11], where only the DFT codebook is used and the joint angle-distance information can be obtained through the received beam pattern. For the second category, some near-field hierarchical beam training schemes were proposed [12], [13], [14]. Specifically, it is performed through the hierarchical codebook with different spatial resolution, where the resolution gradually increases as the searching range gradually decreases during the entire process.

In addition to these two typical schemes, there are other novel low-overhead NFBT schemes. For example, a hashing multi-arm NFBT scheme is proposed in [15], where the multi-arm NFBT codebook is constructed by the random hash functions and the optimal codeword is selected through the soft decision and voting methods. In addition, artificial intelligence (AI) technologies such as neural networks and contrastive learning are also applied in NFBT [16], [17], [18], [19], [20].

However, although the existing NFBT schemes could reduce the training overhead compared to the exhaustive searching scheme, there are still obvious drawbacks that prevent them from achieving near-optimal performance. For the two-phase beam training (TPBT) scheme, the *energy spread* effect will affect the accuracy of the first stage angle searching, thereby further affecting the performance of the overall scheme [8]. For the hierarchical beam training (HBT) scheme, the *error propagation* effect will become more obvious with low SNR and cause serious performance degradation [21]. Consequently, how to address the drawbacks in existing schemes and achieve a near-optimal NFBT scheme with low training overhead is a critical problem, which is however still a blank in the literature.

B. Our Contributions

To fill in this blank, we propose a Bayesian regression (BAR)-based NFBT scheme, which fully utilizes the strong correlation between near-field codewords to achieve near-optimal and low-overhead beam training. Our contributions are summarized as follows:[1]

- We highlight that the received signals corresponding to different near-field beams are highly correlated due to the inherent similarity between channels associated with adjacent locations. This correlation implies that the received signal at the user can provide measurement information not only for its corresponding codeword but also for nearby codewords. Bayesian regression is particularly well-suited to model this correlation and exploit it for efficient codeword selection. Specifically, by modeling the received signal power corresponding to different codewords as a Gaussian process, Bayesian regression allows us to iteratively update the posterior distribution based on real-time feedback from the user. This adaptive approach enables us to strategically select the next codeword to search, thereby reducing the number of required searches compared to exhaustive methods. To the best of our knowledge, this is the first work to apply Bayesian regression [22], [23], [24] to NFBT, and we demonstrate that it can significantly reduce training overhead while maintaining near-optimal performance.
- As described above, the complete process of Bayesian regression can be summarized as modeling the objective function as a random process, reconstructing the objective function by designing a sampling sequence and performing a posterior regression based on a kernel function containing prior information. Therefore, we can set the received signal power corresponding to different codewords as the objective function and model it as a Gaussian process. Then, analyzing the information input from each signal measurement is expected to provide strategic guidance for the next codeword selection, thereby reducing the number of searching required to find the optimal codeword.
- Based on the Bayesian regression, we propose the BAR-based NFBT scheme and provide the overall framework. The key idea is to model the problem of selecting the optimal codeword in NFBT problem as finding the maximum value point of the posterior mean of the reconstructed objective function in Bayesian regression. Specifically, the BS transmits the pilot to the user and iteratively updates the posterior mean, covariance, and variance according to the received signal from user's feedback. In each iteration, different inference strategies correspond to different acquisition functions, where the next searching codeword is determined by maximizing the acquisition function. After completing multiple iterations of searching, the optimal codeword can be determined.
- We analyze and compare different inference strategies, which are particularly important for the overall performance of the proposed scheme. Specifically, we analyze the strengths and drawbacks of the exploitation-based strategy, exploration-based strategy, and exploration-exploitation balanced strategy. Besides, we focus on analyzing the exploration-exploitation balanced strategy, which could significantly balance reducing uncertainty with offering performance improvement. Simulation results demonstrate the efficiency and superiority of the BAR-based NFBT scheme, showing its ability to achieve near-optimal achievable rate performance with low training overhead.

C. Organization and Notation

The remainder of this paper is organized as follows. Section II introduces the system model and the problem formulation. In Section III, two benchmark schemes for NFBT are analyzed, and the challenges and opportunities of the NFBT are discussed. Then the proposed BAR-based NFBT scheme is provided in Section IV. Simulation results are carried out in Section V. Finally, conclusions are drawn in Section VI.

Notation: $\mathbb{C}$ denotes the set of complex numbers; Uppercase and lower-case boldface letters represent matrices and

[1]Simulation codes are provided to reproduce the results in this paper: http://oa.ee.tsinghua.edu.cn/dailinglong/publications/publications.html

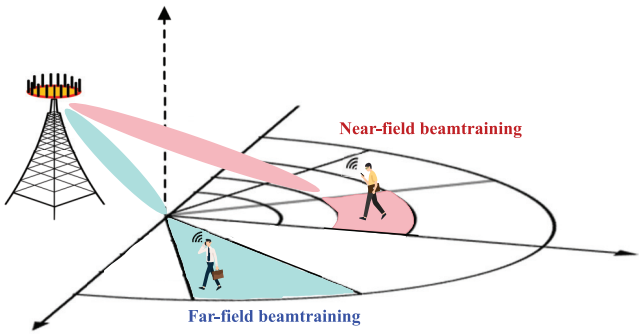

Fig. 1. An illustration of NFBT in XL-MIMO systems.

vectors; $(\cdot)^{-1}, (\cdot)^T, (\cdot)^H$ denote the inverse, transpose, and conjugate transpose, respectively; $|\cdot|$ denotes the absolute operator; $\mathcal{GP}(\boldsymbol{\mu}, \boldsymbol{\Sigma})$ and $\mathcal{CN}(\boldsymbol{\mu}, \boldsymbol{\Sigma})$ denote the Gaussian process and Gaussian distribution with mean $\boldsymbol{\mu}$ and covariance $\boldsymbol{\Sigma}$; $\dim(\cdot)$ represents the dimension of its argument.

II. System Model

In this section, the signal and channel model are first introduced. Next, the NFBT problem is formulated.

A. Signal Model and Channel Model

As illustrated in Fig. 1, a downlink XL-MIMO communication system is considered, where a BS deployed with a N-element uniform linear array (ULA) serves a single-antenna user. The fully-digital precoding structure is adopted where $N_{\mathrm{RF}} = N$ and it could be easily extended to hybrid precoding structure by applying corresponding beam design methods [21], [25], which will be elaborated in Section IV-E.

Let $\mathbf{h} \in \mathbb{C}^{N\times 1}$ denote the downlink channel, and the received signal y_r at the user could be expressed as

$$y_r = \mathbf{h}^H \mathbf{w} s + n, \tag{1}$$

where $\mathbf{w} \in \mathbb{C}^{N\times 1}$ denotes the transmit beamforming vector, s denotes the power-normalized transmitted signal and n denotes the received noise following $\mathcal{CN}\left(0, \sigma^2\right)$. It should be emphasized that since the channel $\mathbf{h}$ is generally determined by the main path, only the direction of the main path needs to be searched by beam training [26]. Therefore, in this paper only the main path is considered, as assumed by [12] and [26].

Generally, the channel model could be separated into the far-field and near-field channel model by the electromagnetic wave propagation characteristics. The Rayleigh distance is usually considered as the boundary, which is defined as $R = \frac{2D^2}{\lambda}$, where D denotes the array aperture and λ represents the carrier wavelength [27]. In XL-MIMO systems, as the number of BS antennas increases, the Rayleigh distance becomes larger accordingly. Therefore, the spherical-wave propagation model should be used to model the near-field channel. Based on the widely-adopted Saleh-Valenzuela model [28], the near-field channel $\mathbf{h}_{\mathrm{n}}$ can be expressed as [8]

$$\mathbf{h}_{\mathrm{n}} = \sqrt{N}\kappa_0 \mathbf{b}(\theta, r), \tag{2}$$

where κ_0 denotes the complex path gain of the line-of-sight (LoS) path, $\mathbf{b}(\theta, r)$ denotes the near-field beam steering vector and $\theta \in [-1, 1]$ denotes the spatial direction. Unlike the far-field beam steering vector focusing the beam energy towards specific directions, the near-field beam steering vector could focus the beam energy on specific locations, which is also called the near-field beam focusing vector [9]. For the ULA, the near-field beam focusing vector $\mathbf{b}(\theta, r)$ can be expressed as

$$\mathbf{b}(\theta, r) = \frac{1}{\sqrt{N}}\left[e^{-jk(r^{(0)}-r)}, \cdots, e^{-jk(r^{(N-1)}-r)}\right]^T, \tag{3}$$

where $k = \frac{2\pi}{\lambda}$ is the wavenumber, $r^{(n)}$ and r denote the distance between the user and the nth element and center of the BS antenna, respectively. The distance $r^{(n)}$ can be expressed as

$$\begin{aligned} r^{(n)} &= \sqrt{r^2 - 2ndr\theta + n^2 d^2} \\ &\overset{(a)}{\approx} r - nd\theta + \frac{n^2 d^2}{2r}(1-\theta^2), \end{aligned} \tag{4}$$

where approximation (a) is the Fresnel approximation, which is derived by $\sqrt{1+x} = 1 + \frac{x}{2} - \frac{x^2}{8} + \mathcal{O}(x^3)$. It has been proven in [6] that the Fresnel approximation (a) is commonly accurate enough when the distance between the user and the BS is larger than $0.5\sqrt{\frac{D^3}{\lambda}}$. It can be obtained from (2) and (3) that the near-field channel is determined by both the angle and the distance of the user.

Before the downlink date transmission, the BS should perform the beam training procedure to ensure that the beam to be transmitted aligns with the main path. The NFBT problem will be formulated as follows.

B. Problem Formulation

For the given beamforming vector $\mathbf{w}$, the achievable rate R can be expressed as

$$R = \log_2\left(1 + \frac{|\mathbf{h}_{\mathrm{n}}^H \mathbf{w}|^2}{\sigma^2}\right). \tag{5}$$

The main purpose of the NFBT is to select the codeword from the predefined codebook to maximize R. The NFBT problem can be expressed as

$$\mathbf{w}^* = \arg\max_{\mathbf{w}\in\mathcal{W}} R, \tag{6}$$

where $\mathcal{W}$ represents the predefined near-field codebook. According to Algorithm 1 in [8], it can be expressed as

$$\mathcal{W} = [\mathbf{b}(\theta_1, r_1^1), \cdots, \mathbf{b}(\theta_1, r_1^{S_1}), \cdots, \mathbf{b}(\theta_N, r_N^{S_N})], \tag{7}$$

where each column of $\mathcal{W}$ corresponds the codeword focusing on a specific position, and S_n denotes the number of sampling distances at θ_n. As illustrated in Fig. 1, unlike the FFBT that only searches the angle of the user, the NFBT searches both the angle and distance. One easy way to solve the NFBT problem (6) is exhaustive scheme. However, due to the additional distance dimension, the training overhead of the exhaustive searching scheme is the product of angle samples and distance samples, i.e., $|\mathcal{W}| = \sum_{n=1}^{N} S_n$, which is unacceptable in practical XL-MIMO systems. Therefore, overhead-reduced NFBT schemes are required and some existing low-overhead benchmark schemes will be introduced as follows.

III. Benchmark Schemes of NFBT

In this section, to reveal the challenges and opportunities of the NFBT, we introduce two typical schemes. Specifically, the near-field TPBT scheme and HBT scheme are introduced at first. Then, the challenges and opportunities of NFBT are discussed.

A. Near-Field TPBT

To reduce the high NFBT overhead of the exhaustive searching scheme, a TPBT scheme is proposed in [10]. In the first phase, the DFT codebook is used to search the optimal angle, which can be expressed as

$$\mathcal{W}_{\mathrm{DFT}} = \left\{ \mathbf{w}_n^{\mathrm{f}} = \mathbf{a}(\theta_n) \right\}, \tag{8}$$

where $\mathbf{a}(\theta_n) = \frac{1}{\sqrt{N}} \left[1, e^{-jkd\theta_n}, \cdots, e^{-jkd(N-1)\theta_n}\right]$. It has been analysed in [10] that the optimal angle θ_{opt} of the first phase can be selected as the middle angle of the dominant angular region. Next, in the second phase, only the codeword corresponding to θ_{opt} need to be searched to get the distance of the user. In addition, the beam training accuracy can be improved by increasing the number of candidate optimal angles K_θ. However, the training overhead also increases with the increase of K_θ. After the two-phase NFBT, the optimal near-field codeword can be gotten.

B. Near-Field HBT

To achieve the trade-off between the overhead and performance, the hierarchical schemes based on near-field hierarchical codebook consisting of several sub-codebooks are proposed [12], [13], [14]. The resolution and size of different sub-codebooks are determined by the angle sampling step Δ_θ and distance sampling step Δ_r. Specifically, as the sampling steps increase, the size of the corresponding sub-codebook becomes smaller and the resolution decreases. The near-field HBT scheme is summarized in Algorithm 1 in [12].

Specifically, the sampling steps of different layers of codebooks gradually decrease through the control parameter $\delta_\Delta (0 < \delta_\Delta < 1)$. Taking the binary-search codebook where $\delta_\Delta = \frac{1}{2}$ as an example, we suppose the angle range and distance range of the k-th sub-codebook $[\theta_{\min}^k, \theta_{\max}^k]$ are $[r_{\min}^k, r_{\max}^k]$, respectively. Then the angle sampling step and distance sampling step in the k-layer and (k+1)-layer codebook are $\Delta_\theta^k = (\theta_{\max}^k - \theta_{\min}^k)/2$, $\Delta_r^k = (r_{\max}^k - r_{\min}^k)/2$, $\Delta_\theta^{k+1} = \Delta_\theta^k/2$ and $\Delta_r^{k+1} = \Delta_r^k/2$, respectively. By searching from the K-layer sub-codebooks in turn, the optimal codeword of the last K-th sub-codebook is selected as the final codeword.

C. Challenges and Opportunities

Challenges: Although the above TPBT and HBT schemes could reduce the training overhead compared to the exhaustive searching scheme, there are still obvious drawbacks limiting their performance. For the TPBT scheme, applying far-field DFT codebook in the first phase may experience significant performance degradation due to the *energy spread* effect [8]. The *energy spread* effect causes that the energy of one near-field path component will be spread into several angles, not centered at one angle, which affects the accuracy of the angle searching, further affecting the performance of the overall scheme. For the HBT scheme, it may suffer from serious performance degradation with low SNR [21]. Specifically, the codewords in higher layers codebooks with wider beamwidth are more susceptible to the noise interference. Once an error judgment occurs in the search of one certain layer of codebook, the "error propagation" will occur, which leads to unrecoverable beam training performance loss.

Opportunities: Both the above two schemes can hardly solve the conflict of reliability and efficiency in NFBT with low SNR. The key issue is that they have not fully utilized the prior knowledge obtained through users' feedback, i.e., the corresponding received signal of the previous transmitted beam. Specifically, the received signal corresponding to different codewords is correlated, thus we can infer the received signal corresponding to other codewords based on the known received signal. Inspired by it, we propose a BAR-based NFBT scheme, which can select the optimal near-field codeword by carefully designing the searching order of codewords and only searching for fewer codewords. It will be analysed in the following section.

IV. Proposed BAR-Based NFBT Scheme

The BAR-based NFBT scheme is proposed in this section. Specifically, the preliminary knowledge of Bayesian regression is introduced first. Then, the proposed BAR-based NFBT scheme is analysed and a overall framework is given. Next, we compare different inference strategies, including exploitation-based, exploration-based and exploration-exploitation balanced strategy. For the exploration-exploitation balanced strategy, three acquisition functions are discussed and analysed. Besides, the computational complexity of the proposed BAR-based NFBT scheme is analysed. Finally, we provide how our proposed BAR-based NFBT scheme can be extended to hybrid precoding structure and multi-user scenarios.

A. Preliminary Knowledge of Bayesian Regression

To reconstruct the objective function $f(\mathbf{x})$ only from few samples, Bayesian regression is widely considered an efficient solution, which can design the sampling order and recover $f(\mathbf{x})$ via its experiential kernels [22]. In this paper, we apply Bayesian regression to achieve efficient codeword selection and NFBT.

Specifically, the objective function $f(\mathbf{x})$ could be modeled as a Gaussian stochastic process $\mathcal{GP}\left(\mu\left(\mathbf{x}\right), k\left(\mathbf{x}, \mathbf{x}'\right)\right)$, where any stochastic process with finite dimensions follows the consistent multivariate Gaussian distribution [29]. It is completely determined by the mean $\mu\left(\mathbf{x}\right)$ and covariance kernel $k\left(\mathbf{x}, \mathbf{x}'\right)$. It should be emphasized that the selection of the kernel functions is crucial for the Bayesian regression process. Without loss of generality, the squared exponential kernel is considered in this paper, which could be expressed as

$$k(\mathbf{x}, \mathbf{x}') = \alpha^2 e^{-\frac{\|\mathbf{x}-\mathbf{x}'\|^2}{\eta^2}}, \tag{9}$$

where α and η are adjustable hyperparameters. It can be obtained from (9) that adjacent sampling points have higher

correlation and the correlation decreases rapidly with increasing distance. Based on (9), the kernel matrix $\mathbf{K}$ could be expressed as

$$\mathbf{K}=\begin{bmatrix} k(\mathbf{x}^1,\mathbf{x}^1) & \cdots & k(\mathbf{x}^1,\mathbf{x}^m) \\ \vdots & \ddots & \vdots \\ k(\mathbf{x}^m,\mathbf{x}^1) & \cdots & k(\mathbf{x}^m,\mathbf{x}^m) \end{bmatrix}. \tag{10}$$

After determining the kernel function, let $\mathbf{y}^t = [y^1,\cdots,y^t]^{\mathrm{T}}$ denote t measurements for samples in $\mathcal{S}^t = \{\mathbf{x}^1,\cdots,\mathbf{x}^t\}$, where $y^i = f(\mathbf{x}^i)+n_i$ and n_i denotes the noise following $n_i \sim \mathcal{CN}\left(0,\sigma^2\right)$. The $f(\mathbf{x})$ and $\mathbf{y}^t$ follow the joint Gaussian distribution, which could be expressed as

$$\begin{bmatrix} f(\mathbf{x}) \\ \mathbf{y}^t \end{bmatrix} \sim \mathcal{CN}\left(\begin{bmatrix} \mu(\mathbf{x}) \\ \boldsymbol{\mu}^t \end{bmatrix}, \begin{bmatrix} k(\mathbf{x},\mathbf{x}') & (\mathbf{k}^t(\mathbf{x}))^{\mathrm{H}} \\ \mathbf{k}^t(\mathbf{x}) & \mathbf{K}^t+\sigma^2\mathbf{I}_t \end{bmatrix}\right), \tag{11}$$

where $\mathbf{k}^t = \left[k\left(\mathbf{x}^1,\mathbf{x}\right),\cdots,k\left(\mathbf{x}^t,\mathbf{x}\right)\right]^{\mathrm{T}}$ and $\boldsymbol{\mu}^t = \left[\mu\left(\mathbf{x}^1\right),\cdots,\mu\left(\mathbf{x}^t\right)\right]^{\mathrm{T}}$. For given $\mathbf{y}^t$, the posterior distribution of $f(\mathbf{x})$ is also a Gaussian process, and its posterior mean, covariance and variance could be obtained by the following lemma.

Lemma 1: For given $\mathbf{y}^t$, the posterior mean, covariance and variance of $f(\mathbf{x})$ could be expressed as

$$\mu^t(\mathbf{x}) = \mu(\mathbf{x}) + \left(\mathbf{k}^t(\mathbf{x})\right)^{\mathrm{H}}\left(\mathbf{K}^t+\sigma^2\mathbf{I}_t\right)^{-1}\left(\mathbf{y}^t-\boldsymbol{\mu}^t\right), \tag{12}$$

$$k^t(\mathbf{x},\mathbf{x}') = k(\mathbf{x},\mathbf{x}') - \left(\mathbf{k}^t(\mathbf{x})\right)^{\mathrm{H}}\left(\mathbf{K}^t+\sigma^2\mathbf{I}_t\right)^{-1}\mathbf{k}^t(\mathbf{x}), \tag{13}$$

$$\sigma^t(\mathbf{x}) = k^t(\mathbf{x},\mathbf{x}). \tag{14}$$

Proof: The proof is provided in Appendix A. ■

Then, the sampling strategy can be formulated based on the posterior mean (12), covariance (13) and variance (14), so the next sampling point can be determined. So far, we have introduced the preliminary knowledge of Bayesian regression and the BAR-based NFBT scheme will be analysed as follows.

B. Proposed BAR-Based NFBT

In NFBT problem, the received signal corresponding to different codewords is highly correlated and the final objective is to find the codeword to maximize the received signal power. Inspired by this, we model the problem of selecting the optimal codeword in NFBT problem as finding the maximum value point of the objective function in Bayesian regression and propose the BAR-based NFBT scheme. Specifically, for different codewords $\mathbf{w}_i$, where $i = 1,2,\cdots,|\mathcal{W}|$, the noiseless received signal vector $\mathbf{g}$ could be expressed as

$$\mathbf{g} = \mathbf{h}^H\mathcal{W}, \tag{15}$$

where $\mathbf{g} \in \mathbb{C}^{1\times|\mathcal{W}|}$, $\mathcal{W} \in \mathbb{C}^{N\times|\mathcal{W}|}$ and $|\mathcal{W}|$ denotes the number of codewords in $\mathcal{W}$ as defined in (7). We can model $\mathbf{g}$ as a Gaussian process $\mathcal{GP}(\mathbf{0}_N,\boldsymbol{\Sigma})$, where $\Sigma \in \mathbb{C}^{|\mathcal{W}|\times|\mathcal{W}|}$ denotes the squared exponential kernel matrix, which could be expressed as

$$\boldsymbol{\Sigma}(i,j) = \alpha^2 e^{-\frac{\|\mathbf{w}_i-\mathbf{w}_j\|^2}{\eta^2}}, \tag{16}$$

where $i,j \in \{1,\cdots,|\mathcal{W}|\}$. Let Ω denote the index of the previous searched codewords, $\mathcal{W}$ denotes the set of all codewords $\mathbf{w}_i$, and $\mathbf{g}_\Omega \in \mathbb{C}^{\dim(\Omega)}$ denotes the corresponding received signal, where $\mathbf{g}_\Omega = \mathbf{g}(\Omega)+\mathbf{n}_\Omega$ with $\mathbf{n}_\Omega \sim \mathcal{CN}(\mathbf{0}_{\dim(\Omega)},\sigma^2\mathbf{I}_{\dim(\Omega)})$. Therefore, similar to (11), the joint distribution of $\mathbf{g}$ and $\mathbf{g}_\Omega$ could be expressed as

$$\begin{bmatrix} \mathbf{g} \\ \mathbf{g}_\Omega \end{bmatrix} \sim \mathcal{CN}\left(\begin{bmatrix} \mathbf{0}_N \\ \mathbf{0}_{\dim(\Omega)} \end{bmatrix}, \begin{bmatrix} \boldsymbol{\Sigma} & \boldsymbol{\Sigma}(:,\Omega) \\ \boldsymbol{\Sigma}(\Omega,:) & \boldsymbol{\Sigma}(\Omega,\Omega)+\sigma^2\mathbf{I}_{\dim(\Omega)} \end{bmatrix}\right). \tag{17}$$

Thus, for given $\mathbf{g}_\Omega$, the posterior mean $\boldsymbol{\mu}_\Omega$, covariance $\boldsymbol{\Sigma}_\Omega$ and variance $\boldsymbol{\sigma}_\Omega$ can be obtained according to Lemma 1:

$$\boldsymbol{\mu}_\Omega = \boldsymbol{\Sigma}(:,\Omega)\left(\boldsymbol{\Sigma}(\Omega,\Omega)+\sigma^2\mathbf{I}_{\dim(\Omega)}\right)^{-1}\mathbf{g}_\Omega, \tag{18}$$

$$\boldsymbol{\Sigma}_\Omega = \boldsymbol{\Sigma} - (\boldsymbol{\Sigma}(\Omega,:))^{\mathrm{H}}\left(\boldsymbol{\Sigma}(\Omega,\Omega)+\sigma^2\mathbf{I}_{\dim(\Omega)}\right)^{-1}\boldsymbol{\Sigma}(\Omega,:), \tag{19}$$

$$\boldsymbol{\sigma}_\Omega = \boldsymbol{\Sigma}_\Omega(n,n). \tag{20}$$

To summarize, the flowchart and overall framework of the proposed BAR-based NFBT scheme is shown in Fig. 2 and Algorithm 1, respectively. Specifically, the BS selects the codeword and transmits the corresponding pilot signal. For the first codeword, it is randomly selected. Then, the UE updates the received signal $\mathbf{g}_\Omega$ and reports the data feedback to the BS. It should be noted that the feedback data in proposed scheme is actual value not a binary sequence. Next, the BS can update the posterior mean $\boldsymbol{\mu}_\Omega$, covariance $\boldsymbol{\Sigma}_\Omega$, variance $\boldsymbol{\sigma}_\Omega$ and determine the next codeword based on the inference strategy. Specifically, different inference strategies correspond to different acquisition functions $V(\boldsymbol{x})$, which determine the searching sequence of codewords and the accuracy of the posterior predictive distribution in Bayesian regression [30]. The acquisition functions serve as critical tools that guide the optimization process by quantifying the utility of potential input points for sampling. In each iteration, the next codeword is determined by maximizing the acquisition function, i.e.,

$$\boldsymbol{x}_{t+1} = \underset{\boldsymbol{x}\in\mathcal{W}/\Omega_t}{\operatorname{argmax}}\ V(\boldsymbol{x}), \tag{21}$$

Algorithm 1 Overall Framework of the Proposed BAR-Based NFBT

Inputs: Near-field polar-domain codebook $\mathcal{W}$, kernal matrix $\boldsymbol{\Sigma}$, number of pilots $T_{\max}$.
Output: Optimal codeword $\mathbf{w}^*$.
1: Initialization: $\Omega = \oslash$.
2: **for** $t = 1,2,\cdots,T_{\max}$ **do**
3: Received signal power update: $\mathbf{g}_\Omega = \mathbf{g}(\Omega)+\mathbf{n}_\Omega$.
4: Posterior mean $\boldsymbol{\mu}_\Omega$, covariance $\boldsymbol{\Sigma}_\Omega$ and variance $\boldsymbol{\sigma}_\Omega$ update according to (18), (19) and (20).
5: Determine the next codeword by maximizing the acquisition function $V(\boldsymbol{x})$ according to the inference strategy: $\boldsymbol{x}_{t+1} = \underset{\boldsymbol{x}\in\mathcal{W}/\Omega_t}{*argmax}\ V(\boldsymbol{x})$.
6: Index of searched codewords update: $\Omega_t \cup \boldsymbol{x}_{t+1}$.
7: **end for**
8: Determine the index of the optimal codeword based on the maximum point of $\boldsymbol{\mu}_\Omega$ and select corresponding codeword as the optimal codeword $\mathbf{w}^*$.
9: **return:** Optimal codeword $\mathbf{w}^*$.

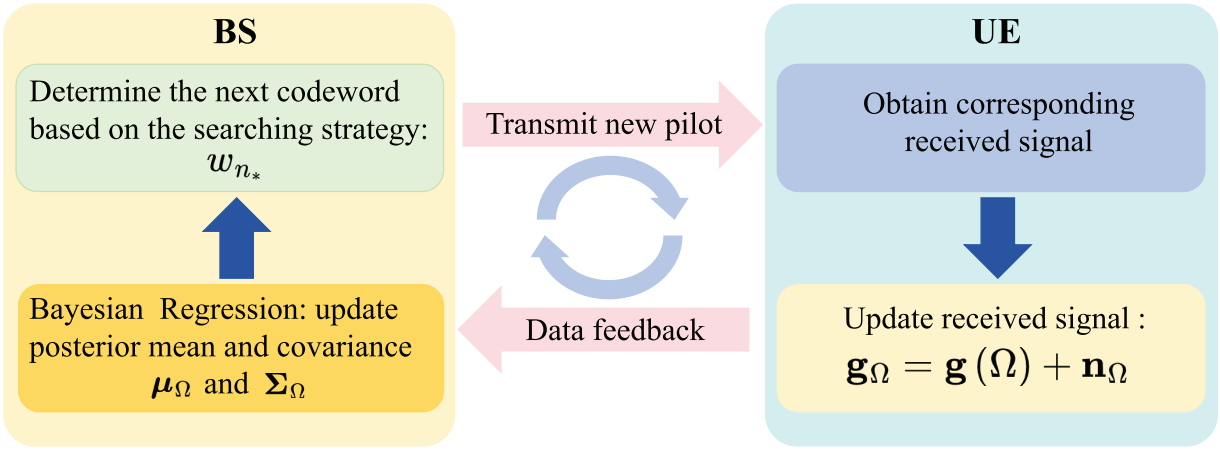

Fig. 2. A flowchart of the BAR-based NFBT scheme.

Searching Strategy	Diagram	Strengths	Drawbacks
exploitation-based strategy	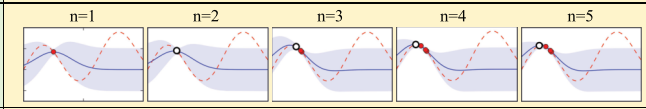	The searching strategy corresponds to our target, which can quickly obtain the extreme point	Have the risk of plunging into a local optimal solution
exploration-based strategy	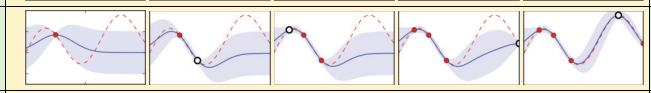	Gradually reduce the uncertainty and prevent plunging into a local optimal solution	Search for many "worthless points" and increase search overhead
exploration-exploitation balanced strategy	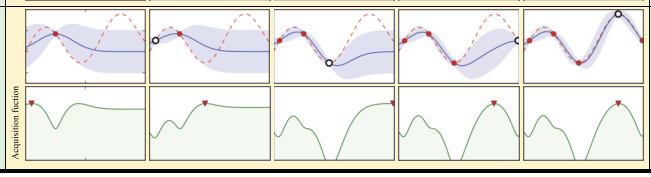	Achieve a perfect tradeoff between reducing uncertainty and offering improvement over the current best observation	

Fig. 3. Comparison between different inference strategies of the proposed BAR-based NFBT scheme.

where / denotes the set difference. For the iteration, Ω_t can be updated by $\Omega_t \cup \boldsymbol{x}_{t+1}$. By maximizing the acquisition function, we can strategically select the next input point that is expected to yield the most informative or beneficial outcome, thereby enhancing the efficiency of the optimization process.

In summary, the main advantage of our proposed BAR-based NFBT scheme is its ability to efficiently exploit the correlation between codewords and adaptively refine the search process. This leads to a significant reduction in training overhead while maintaining near-optimal performance. It should be emphasized that selecting the appropriate inference strategy is particularly important for the overall performance of the BAR-based NFBT scheme, which will be discussed as follows.

C. Comparison Between Different Searching Strategies

In this subsection, different inference strategies of the proposed BAR-based NFBT scheme are analysed and compared. Without loss of generality, we define $\mathbf{G}_{\Omega_T} = [\mathbf{g}_{\Omega_1}, \mathbf{g}_{\Omega_2}, \cdots, \mathbf{g}_{\Omega_T}]$, where $\mathbf{g}_{\Omega_t} = \mathbf{g}(\mathbf{w}_t) + n_t$, $n_t \sim \mathcal{CN}\left(0, \sigma^2\right)$, $\mathbf{w}_t$ denotes the selected codeword at time slot t and $T < |\mathcal{W}|$. For simplicity, we use $\boldsymbol{x}_t$ to represent $\mathbf{w}_t$. As discussed before, the inference strategy is the key factor affecting the performance of the BAR-based NFBT scheme. For clarity, in Fig. 3 we summarize three different inference strategies, whose details are analysed as follows.

1) Exploitation-based Strategy: The objective of NFBT is to select codeword which maximizes the user's received signal power. In other words, we only need to determine the maximum value point of the posterior mean of the reconstructed objective function $\mathbf{g}_\Omega$ and select its corresponding codeword without accurately reconstructing the entire objective function [22]. Thus, the exploitation-based inference strategy can be directly applied, which focuses on exploiting the already known high-performing regions.

For the exploitation-based inference strategy, the acquisition function $V^{\text{exploit}}(\boldsymbol{x})$ could be expressed as

$$V^{\text{exploit}}(\boldsymbol{x}) = \mu_{\boldsymbol{x}}. \tag{22}$$

Therefore, the exploitation-based inference strategy can be expressed as

$$\boldsymbol{x}_{t+1} = \underset{\boldsymbol{x}\in\mathcal{W}/\Omega_t}{\operatorname{argmax}}\ V_t^{\text{exploit}}(\boldsymbol{x}) = \underset{\boldsymbol{x}\in\mathcal{W}/\Omega_t}{\operatorname{argmax}}\ \mu_t(\boldsymbol{x}), \tag{23}$$

where $\Omega_t = \{\boldsymbol{x}_1, \ldots, \boldsymbol{x}_t\}$ and $\mathcal{W}$ denotes the set of all $\boldsymbol{x}_t$. Thus, we can update Ω_t by $\Omega_t \cup \boldsymbol{x}_{t+1}$ and iterate the process until selecting the optimal codeword. The main strength of this exploitation-based strategy is that it may obtain the extreme

point quickly. However, it may face the risk of obtaining a local optimal solution.

2) Exploration-based Strategy: Another strategy to select the optimal codeword is to first globally reconstruct the objective function, then determine the estimated maximum value point of the posterior mean of the objective function and choose its corresponding codeword [31]. Thus, the exploration-based inference strategy can be applied, which tends to search the regions of high uncertainty. In other words, its goal is to reconstruct the entire unknown objective function as accurately and quickly as possible, which is called *Gaussian process active learning* [24].

Specifically, to reduce the uncertainty of the estimated objective function, the main objective is to maximize the mutual information (or the information gain) between $\mathbf{g}$ and $\mathbf{g}_\Omega$ [32], which could be expressed as

$$\begin{aligned}\max I(\mathbf{g}_\Omega;\mathbf{g}) &= \mathrm{H}(\mathbf{g}_\Omega) - \mathrm{H}(\mathbf{g}_\Omega|\mathbf{g}) \\ &= \log\left|\mathbf{I}_{\dim(\Omega)} + \frac{1}{\sigma^2}\boldsymbol{\Sigma}_\Omega\right|, \end{aligned} \tag{24}$$

where $\mathrm{H}(\cdot)$ denotes the entropy and for a Gaussian distribution, $\mathrm{H}(N(\mu,\Sigma)) = \frac{1}{2}\log|2\pi e\Sigma|$. However, solving the problem (24) is NP-hard. We can use the Gaussian process regression (GPR) based algorithm to approximate the solution [31]. Specifically, we set $F(\Omega) = I(\mathbf{g}_\Omega;\mathbf{g})$ and set the posterior variance as the acquisition function of the exploration-based inference strategy, which can be expressed as

$$V^{\text{explore}}(\boldsymbol{x}) = \boldsymbol{\sigma}_{\boldsymbol{x}}. \tag{25}$$

Therefore, the exploration-based inference strategy can be expressed as

$$\boldsymbol{x}_{t+1} = \underset{\boldsymbol{x}\in\mathcal{W}/\Omega_t}{\operatorname{argmax}}\ V_t^{\text{explore}}(\boldsymbol{x}) = \underset{\boldsymbol{x}\in\mathcal{W}/\Omega_t}{\operatorname{argmax}}\ \sigma_t(\boldsymbol{x}), \tag{26}$$

where $\Omega_t = \{\boldsymbol{x}_1,\ldots,\boldsymbol{x}_t\}$. The main strength of this exploration-based strategy is that it can reconstruct the entire objective function accurately and quickly by gradually reducing the uncertainty which prevents plunging into a local optimal solution. However, it may search for many "worthless points" and increase training overhead.

3) Exploration-exploitation Balanced Strategy: Based on the above analysis, a exploration-exploitation balanced strategy should be adopted, which can dynamically trade off between bringing performance improvement and reducing uncertainty when determining the next codeword. Thus, corresponding acquisition function $V^{\text{balanced}}(\boldsymbol{x})$ of the exploration-exploitation balanced strategy should be determined and three effective functions are discussed as follows.

A) Probability of improvement (PI): A typical acquisition function of the exploration-exploitation balanced strategy is called *probability of improvement* [33], which could be expressed as

$$\begin{aligned}\mathrm{PI}(\boldsymbol{x}) &= P(\mathbf{g}(\boldsymbol{x}) \geq \mathbf{g}(\boldsymbol{x}_{\max}) + \xi) \\ &= \Phi\left(\frac{\mu_{\boldsymbol{x}} - \mathbf{g}(\boldsymbol{x}_{\max}) - \xi}{\boldsymbol{\sigma}_{\boldsymbol{x}}}\right), \end{aligned} \tag{27}$$

where $\Phi(\cdot)$ denotes the normal cumulative distribution function (CDF), $\mathbf{g}(\boldsymbol{x}_{\max}) = \underset{\boldsymbol{x}_i\in\Omega_t}{\operatorname{argmax}}\ \mathbf{g}(\boldsymbol{x}_i)$, and ξ denotes the adjustable trade-off parameter. It is recommended in [33] that ξ should decrease gradually throughout the entire search process. Specifically, when ξ is enough high early, it tends to search the regions of high uncertainty and the exploration-based strategy dominates. When ξ becomes 0, the exploration-exploitation balanced strategy is transformed into the exploitation-based strategy.

B) Expected improvement (EI): Another acquisition function of the exploration-exploitation balanced strategy is *expected improvement*, which considers both the probability and degree of the improvement [34]. Specifically, the EI acquisition function could be expressed as

$$\mathrm{EI}(\boldsymbol{x}) = \begin{cases}(\mu_{\boldsymbol{x}} - \mathbf{g}(\boldsymbol{x}_{\max}) - \xi)\Phi(Z) + \boldsymbol{\sigma}_{\boldsymbol{x}}\phi(Z), & \boldsymbol{\sigma}_{\boldsymbol{x}} > 0 \\ 0, & \boldsymbol{\sigma}_{\boldsymbol{x}} = 0, \end{cases} \tag{28}$$

where

$$Z = \begin{cases}\frac{\mu_{\boldsymbol{x}} - \mathbf{g}(\boldsymbol{x}_{\max}) - \xi}{\boldsymbol{\sigma}_{\boldsymbol{x}}}, & \boldsymbol{\sigma}_{\boldsymbol{x}} > 0 \\ 0, & \boldsymbol{\sigma}_{\boldsymbol{x}} = 0, \end{cases} \tag{29}$$

$\Phi(\cdot)$ and $\phi(\cdot)$ represent the CDF and probability density function (PDF) of the standard normal distribution and ξ is the adjustable trade-off parameter like in (27). Besides, it has been proven that setting $\xi = 0.01$ can achieve good performance in most cases [35].

C) Gaussian process upper confidence bound (GP-UCB): Additionally, GP-UCB is widely used as the acquisition function, which measures the quality of the codeword searching process by quantifying regret [31]. Specifically, the goal of BAR-based NFBT is to select the codeword which maximizes corresponding received signal power, i.e.,

$$\boldsymbol{x}^* = \underset{\boldsymbol{x}\in\mathcal{W}}{\operatorname{argmax}}\ \mathbf{g}(\boldsymbol{x}), \tag{30}$$

where $\boldsymbol{x}^*$ denotes the optimal codeword. One equivalent method for (30) is to minimize the cumulative regret, which could be expressed as

$$R_T = \sum_{t=1}^{T} r_t, \tag{31}$$

where $r_t = \mathbf{g}(\boldsymbol{x}^*) - \mathbf{g}(\boldsymbol{x}_t)$. However, solving (30) or minimizing the cumulative regret is NP-hard. Thus, GP-UCB can be applied as the acquisition function, which could be expressed as

$$\text{GP–UCB}(\boldsymbol{x}) = \mu_{t-1}(\boldsymbol{x}) + \sqrt{\beta_t}\sigma_{t-1}(\boldsymbol{x}), \tag{32}$$

where β_t is an adjustable hyperparameter, which balances exploration and exploitation. Besides, β_t is usually set as: $\beta_t = 2\log(|\mathcal{W}|t^2\pi^2/6\delta)$, where $\delta \in (0,1)$ [31]. Different from the classical multi-armed bandit problem [36], the regrets of the GP-UCB is highly correlated to the kernel matrix $\boldsymbol{\Sigma}$. It can be proven that the cumulative regret of GP-UCB algorithm is bounded and sublinear for T by the following lemma, which means each round of regret could gradually decrease to choose the better point.

Lemma 2: For the Gaussian process $\mathbf{g}$ with mean zero and covariance kernel $k(\mathbf{x},\mathbf{x}')$, applying GP-UCB algorithm with $\beta_t = 2\log(|\mathcal{W}|t^2\pi^2/6\delta)$ could obtain a regret

bound $\mathcal{O}^*(\sqrt{T\gamma_T \log|\mathcal{W}|})$ with high probability, which can be expressed as

$$\Pr\left\{R_T \leq \sqrt{\frac{8T\beta_T\gamma_T}{\log(1+\sigma^{-2})}}\right\} \geq 1-\delta, \tag{33}$$

where $\delta \in (0,1)$ and γ_T denotes the maximum information gain after T rounds, i.e.,

$$\gamma_T = \max_{\Omega_T \subset \mathcal{W}, |\Omega_T|=T} I(\mathbf{g}_{\Omega_T}; \mathbf{g}_T). \tag{34}$$

Proof: The proof is provided in Appendix B. ■

Therefore, based on Lemma 2, it could be concluded that the GP-UCB algorithm has sublinear bound on cumulative regret with high probability, which also means the GP-UCB algorithm is *no regret* with high probability, i.e., $\lim_{T\to\infty}\frac{R_T}{T}=0$. It should be noted that γ_T depends on the form of kernel and it has been proven the squared exponential kernel is sublinear for T [22].

So far, we have analyzed our proposed BAR-based NFBT scheme and compared different inference strategies based on distinct acquisition functions. Simulation results are carried out to substantiate the efficacy and superiority of the BAR-based NFBT scheme in the following section.

D. Computational Complexity of BAR-Based NFBT Scheme

In this subsection, we will analyse the computational complexity of proposed BAR-based NFBT scheme. Specifically, the entire signal processing of the BAR-based NFBT scheme is composed of iterative update of the acquisition function $V(x)$ and selecting optimal codeword after the iteration. For the iterative update of $V(x)$, the computational complexity is determined by the calculation of posterior variance. According to (19), (20), and (32), its computational complexity is $\mathcal{O}\left(T^2\left(T^2+|\mathcal{W}|T+|\mathcal{W}|^2\right)\right)$. For selecting optimal codeword after the iteration, the computational complexity is $\mathcal{O}\left(|\mathcal{W}|T\right)$.

It should be noted that although the computational complexity of iterative update of the acquisition function $V(x)$ is relatively high, it can be carried out offline in advance. Then, the corresponding calculated posterior mean $\boldsymbol{\mu}_\Omega$, covariance $\boldsymbol{\Sigma}_\Omega$ and variance $\boldsymbol{\sigma}_\Omega$ can be saved at the BS for the optimal codeword selection stage. Besides, as the iterative update of the acquisition function $V(x)$ isn't determined by the specific user, the optimal codeword selection can work parallel. These confirm the practicality of our proposed BAR-based NFBT scheme. Besides, beam training overhead generally refers to the number of time slots used for beam training and the training overhead of different schemes is compared in subsection V-C.

E. Extension to Hybrid Precoding Structure and Multi-User Scenarios

In this subsection, we will demonstrate how our proposed BAR-based NFBT scheme can be extended to hybrid precoding structure and multi-user scenarios.

1) Extension to Hybrid Precoding Structure: For the hybrid precoding structure, the number of RF chains N_{RF} is usually much smaller than the number of BS antennas N, i.e., $N_{\mathrm{RF}} \ll N$. In short, the optimization of hybrid precoding can be decomposed into analog and digital precoding design. For analog precoding, the training process is similar to the fully-digital structure and the differences lies in that the codewords should be generated in hybrid structure and they meet the requirements of envelop constraint. Besides, there are already several schemes for analog codewords design [25], [37], [38]. After getting the analog precoding, the digital precoding can be obtained through several schemes, such as zero-forcing (ZF) [39] and weighted minimum mean square error (WMMSE) [40].

2) Extension to Multi-User Scenarios: For simplicity, the single-user scenarios is considered in this paper. It is worth noting that our proposed BAR-based NFBT scheme is also suitable for multi-user scenarios. For our proposed BAR-based NFBT scheme, the codewords generation and selection process is independent of UE. Thus different users can independently perform the BAR-based NFBT process with the BS as described in Fig. 2.

V. Simulation Results

In this section, simulation results are carried out to substantiate the performance of the BAR-based NFBT scheme. Specifically, the simulation setup is first introduced. Then, the performance of Bayesian regression applied in NFBT is presented. Besides, the overhead and performance of different schemes are compared.

A. Simulation Setup

We set the number of the BS antennas as $N = 256$. Besides, we set the carrier frequency as 30 GHz and the antenna spacing is $d = \frac{\lambda}{2} = 0.5$ cm. For simplicity, the single-user scenario is considered, i.e., the number of users is $K = 1$. For the user distribution, the user is randomly distributed in a sector, where the spatial angle range and distance range are $\left[-\frac{\pi}{3}, \frac{\pi}{3}\right]$ and $[8\ \mathrm{m}, 80\ \mathrm{m}]$, respectively. Besides, the monte-carlo simulation is carried out and its number is set to $N_{\mathrm{iter}} = 500$. The complex path gain of the LoS path is $\kappa_0 \sim \mathcal{CN}(0,1)$.

Moreover, for the BAR-based NFBT scheme, we set the hyperparameters of the squared exponential kernel as $\alpha^2 = 1$ and $\eta^2 = \frac{2}{\Delta_{\mathrm{loc}}}$, where $\Delta_{\mathrm{loc}} = \sqrt{\Delta_\theta^2 + \frac{1}{\Delta_r^2}}$, Δ_θ and Δ_r denote the angle and distance sampling steps of the polar-domain codebook. It should be emphasized selecting the appropriate hyperparameters is particularly important for the performance of the BAR-based NFBT scheme as they affect the correlation between different near-field codewords. The optimal hyperparameters could be obtained by the maximum likelihood (ML) criterion [41] and only a value with good performance is set here. Besides, for the PI and EI acquisition function of the exploration-exploitation balanced strategy, we set $\xi = 0.01$ [35]. For the GP-UCB acquisition function, we set $\delta = 0.1$ of β_t.

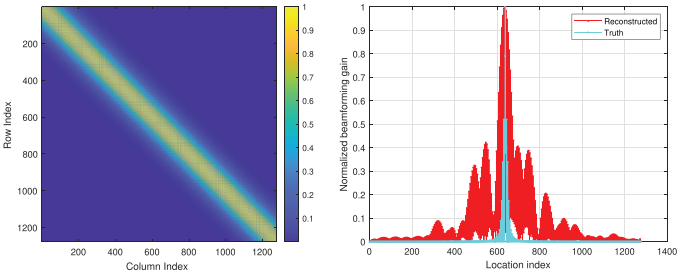

(a) The exponential kernel matrix (b) Normalized beamforming gain

Fig. 4. The performance of Bayesian regression applied in NFBT.

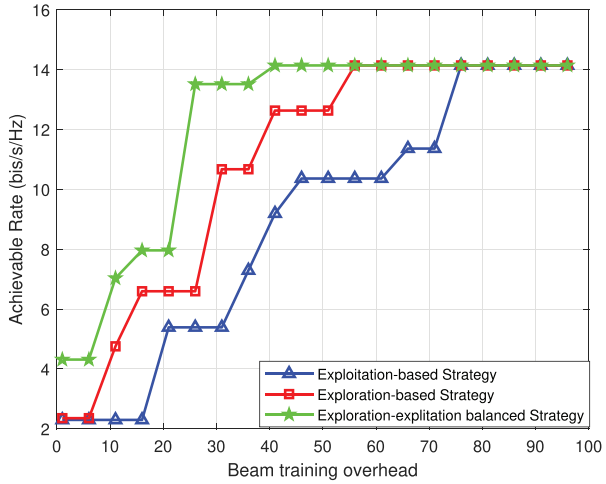

Fig. 5. Performance comparison of the BAR-based NFBT scheme with different searching strategies.

B. The Performance of Bayesian Regression Applied in NFBT

The performance of Bayesian regression applied in NFBT is evaluated in this subsection. The considered exponential kernel matrix is plotted in Fig. 4(a) and the normalized beamforming gain corresponding to different codewords is plotted in Fig. 4. Specifically, we suppose that the angle and distance of the user are $\theta = 0$ and $r = 15$ m, respectively. The blue line denotes the true normalized beamforming gain and the red line denotes the reconstructed normalized beamforming gain through Bayesian regression. Different from the problems like channel estimation in [29] which require fast and accurate reconstruction of the objective function, we only need to determine the maximum value point of the posterior mean of the reconstructed objective function and select its corresponding codeword in NFBT. As shown in Fig. 4, although there are deviations between the true and reconstructed normalized beamforming gain, the maximum value point can still be accurately determined to select the optimal codeword.

To evaluate the different searching strategies mentioned in subsection IV-C, we compare the performance of the BAR-based NFBT scheme with different searching strategies in Fig. 5. It can be shown that the performance of applying the exploration-exploitation balanced strategy will be superior to applying the other two strategies, which confirms the strengths and drawbacks of the different strategies analyzed and summarized in subsection IV-C.

TABLE I
COMPARISON OF BEAM TRAINING OVERHEAD

Schemes	Overhead	Value
Far-field exhaustive searching scheme	N	256
Near-field exhaustive searching scheme	NS	1280
Near-field TPBT scheme [10]	$N+S$	261
Near-field HBT scheme [12]	$\sum_l^L N^{(l)}S^{(l)}$	393
Proposed BAR-based NFBT scheme		50

C. Comparison of the Beam Training Overhead

In Table. I, the training overhead of different schemes is compared. Beam training overhead usually refers to the number of time slots or searched codewords.[2] We compare the BAR-based NFBT scheme with far-field exhaustive searching scheme, near-field exhaustive searching scheme, near-field TPBT scheme [10] and near-field HBT scheme [12]. Specifically, the number of sampled angles and distances are $N = 256$ and $S = 5$. For the exhaustive searching schemes, the far-field and near-field training overhead are 256 and $256 \times 5 = 1280$, respectively. Besides, the training overhead of the near-field TPBT scheme is $256 + 5 = 261$. Moreover, for the near-field HBT scheme, the training overhead is $\mathcal{O}\left(log\left(N\right) + log\left(S\right)\right)$. In this paper, we use two-layer hierarchical scheme, where the control parameter of the sampling steps is set to $\delta_\Delta = 0.5$. Let $N^{(l)}$ and $S^{(l)}$ denote the number of sampled angles and distances in the l-th layer searching, respectively. Thus, the training overhead of the near-field HBT scheme is $N^{(1)}S^{(1)} + N^{(2)}S^{(2)} = 128 \times 3 + 3 \times 3 = 393$. For the BAR-based NFBT scheme, the training overhead can be dynamically adjusted. To demonstrate the advantages of the BAR-based NFBT scheme over the benchmark schemes, we set it to a constant value. Compared to the near-field exhaustive searching scheme, it could reduce almost 96% of the overhead.

Besides, the achievable rate performance of different schemes against the training overhead is shown in Fig. 6, where SNR = 10 dB. It can be shown that the BAR-based NFBT scheme only needs 50 overhead to almost achieve the performance of the near-field exhaustive searching scheme. For the near-field TPBT and HBT scheme, their beam training overhead are still strongly related to the size of the codebook and are usually unacceptable when the size of the codebook in XL-MIMO systems is large. For our proposed scheme, it can perform well with low overhead. This is because it fully utilizes the correlation between different codewords and when the number of transmitting pilots increases, the reconstructed objective function in Bayesian regression becomes more accurate and the optimal codeword can be quickly determined.

D. Comparison of the Beam Training Performance

First, the achievable rate performance of different schemes against the SNR is plotted in Fig. 7. Specifically, it can be shown that the BAR-based NFBT scheme can almost achieve

[2]In subsection V-C and V-D, based on the comparison of different searching strategies above, we adopt the exploration-exploitation balanced strategy and select GP-UCB as the acquisition function for the BAR-based NFBT scheme.

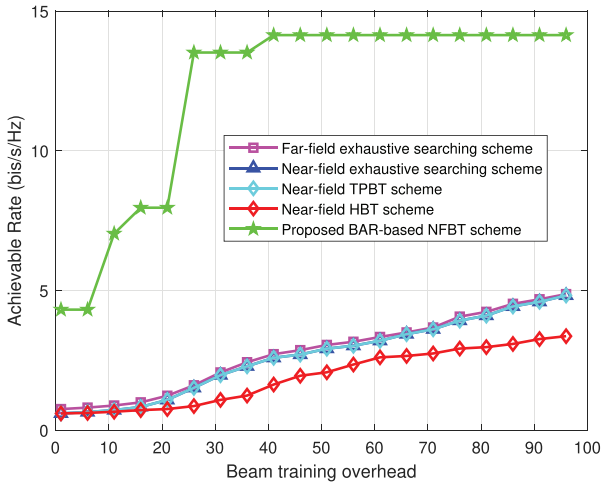

(a)

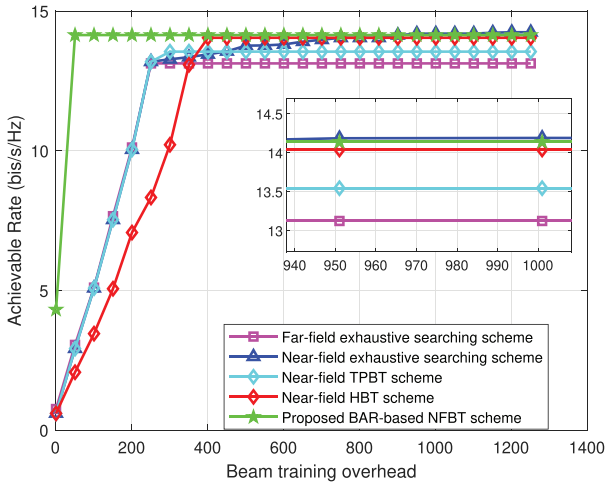

(b)

Fig. 6. Achievable rate performance vs. the beam training overhead.

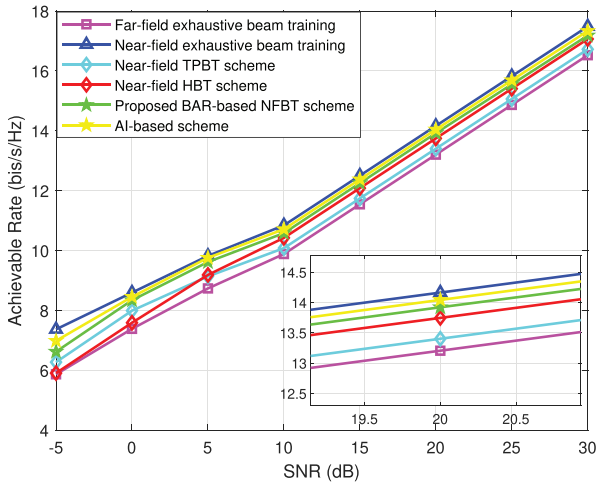

(a)

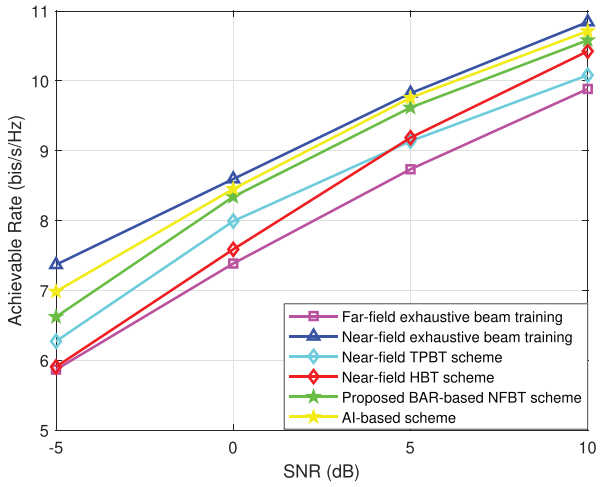

(b)

Fig. 7. Achievable rate performance vs. the SNR.

the performance of the near-field exhaustive searching scheme and outperform the near-field TPBT and HBT scheme. For the TPBT scheme in [10], as it applies DFT codebook in the first phase, the *energy spread* effect affects the accurracy of angle searching and causes the performance loss. For the near-field HBT scheme in [12], as the wide beam is easily affected by noise, it faces the serious performance degradation at low SNR. The proposed scheme can exclude the influence of the above two factors and perform well. Additionally, we compared our proposed BAR-based NFBT scheme with AI-based methods in [18]. Although the AI-based scheme performs well, it require extensive training data and computational resources. In contrast, our proposed BAR-based scheme leverages the inherent correlation between near-field codewords, providing a more efficient alternative that is particularly suitable for practical implementation in extremely large-scale MIMO systems.

Besides, the achievable rate performance of different schemes against the distance of the user from the BS is shown in Fig. 8, where the spatial direction of the user is $\theta = 0$ and SNR = 10 dB. It can be shown that as the distance increases the performance of the BAR-based NFBT scheme almost remains unchanged, which confirms the universality and effectiveness of the BAR-based NFBT scheme in both near-field and far-field scenarios. In contrast, for the near-field TPBT scheme

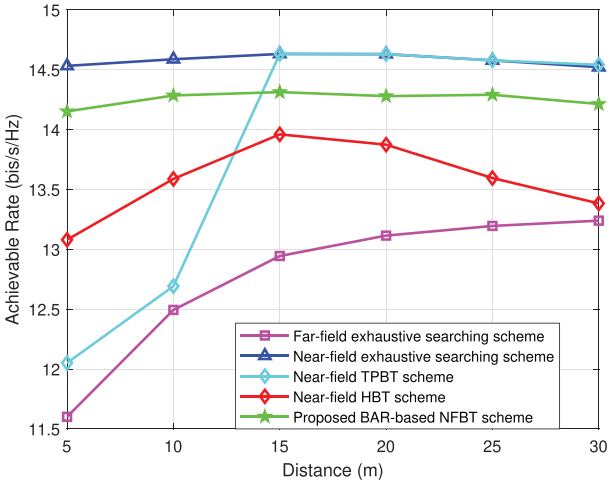

Fig. 8. Achievable rate performance vs. the distance.

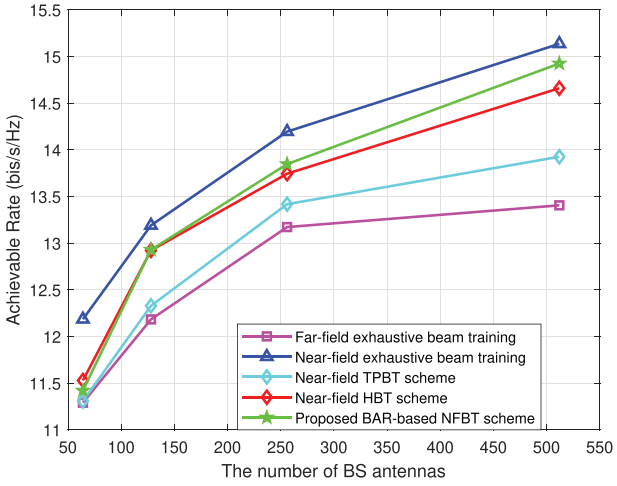

Fig. 9. Achievable rate performance vs. the number of BS antennas N.

in [10], its achievable rate performance gradually decreases with the distance decreasing and it has poor performance when the user is close to the BS. This is because the performance of the near-field TPBT scheme is highly dependent on the accuracy of the first phase angle searching, which is influenced by the *energy spread* effect. Specifically, it has been proven in [11] that with the distance decreasing, the *energy spread* effect becomes more pronounced, which in turn affects the accuracy of angle searching. In other words, the near-field TPBT scheme still applies the far-field DFT codebook to determine the angle of the user in the first phase. With the distance decreasing and the near-field propagation becoming more dominant, the far-field DFT codebook and near-field model become increasingly mismatched, which causes increasingly performance loss. For the near-field HBT scheme in [12], its performance is almost unaffected by user's distance changing but still easily affected by noise.

Furthermore, the achievable rate performance of different schemes against the number of BS antennas N is shown in Fig. 9, where SNR = 10 dB. It can be shown that the proposed BAR-based NFBT scheme outperforms the benchmark schemes under different number of BS antennas N settings. This confirms the universality of the BAR-based NFBT scheme.

VI. Conclusion

In this paper, we first apply Bayesian regression into NFBT and propose the BAR-based NFBT scheme. Different from the existing NFBT schemes, the proposed scheme models the problem of selecting the optimal codeword as finding the maximum value point of the posterior mean of the objective function in Bayesian regression, which fully utilized the correlation between near-field codewords to reduce the training overhead. Simulation results confirm that the efficiency of the BAR-based NFBT scheme, which only requires searching for few codewords instead of the entire codebook to select the optimal codeword. For the future research, Bayesian regression may be applied in other scenarios of near-field communications, such as channel estimation [42] and beam tracking [43]. Low-overhead NFBT schemes of the extremely large-scale reconfigurable intelligent surface (XL-RIS) may also be a critical future research direction [44].

Appendix A
Proof of Lemma 1

Based on (11), the joint PDF of $f(\mathbf{x})$ and $\mathbf{y}^t$ could be expressed as

$$p(f(\mathbf{x}),\mathbf{y}^t) = \mathcal{CN}\left(\begin{bmatrix}\mu(\mathbf{x})\\ \boldsymbol{\mu}^t\end{bmatrix},\begin{bmatrix}k(\mathbf{x},\mathbf{x}') & (\mathbf{k}^t(\mathbf{x}))^{\mathrm{H}}\\ \mathbf{k}^t(\mathbf{x}) & \mathbf{K}^t+\sigma^2\mathbf{I}_t\end{bmatrix}\right). \tag{35}$$

According to Bayes theorem, the joint PDF $p(f(\mathbf{x}),\mathbf{y}^t)$ could also be expressed as

$$p(f(\mathbf{x}),\mathbf{y}^t) = p(f(\mathbf{x})|\mathbf{y}^t)p(f(\mathbf{y}^t)). \tag{36}$$

First, the covariance matrix could be decomposed as follows

$$\begin{bmatrix}k(\mathbf{x},\mathbf{x}') & (\mathbf{k}^t(\mathbf{x}))^{\mathrm{H}}\\ \mathbf{k}^t(\mathbf{x}) & \mathbf{K}^t+\sigma^2\mathbf{I}_t\end{bmatrix} = \begin{bmatrix}1 & \mathbf{U}\\ 0 & 1\end{bmatrix}\begin{bmatrix}\mathbf{V} & 0\\ 0 & \mathbf{K}^t+\sigma^2\mathbf{I}_t\end{bmatrix}\begin{bmatrix}1 & 0\\ \mathbf{W} & 1\end{bmatrix}, \tag{37}$$

where

$$\mathbf{U} = (\mathbf{k}^t(\mathbf{x}))^{\mathrm{H}}(\mathbf{K}^t+\sigma^2\mathbf{I}_t)^{-1}. \tag{38}$$

$$\mathbf{V} = k(\mathbf{x},\mathbf{x}') - (\mathbf{k}^t(\mathbf{x}))^{\mathrm{H}}(\mathbf{K}^t+\sigma^2\mathbf{I}_t)^{-1}\mathbf{k}^t(\mathbf{x}). \tag{39}$$

$$\mathbf{W} = (\mathbf{K}^t+\sigma^2\mathbf{I}_t)^{-1}\mathbf{k}^t(\mathbf{x}). \tag{40}$$

Based on (37), we can get

$$\begin{aligned}&\begin{bmatrix}k(\mathbf{x},\mathbf{x}') & (\mathbf{k}^t(\mathbf{x}))^{\mathrm{H}}\\ \mathbf{k}^t(\mathbf{x}) & \mathbf{K}^t+\sigma^2\mathbf{I}_t\end{bmatrix}^{-1}\\ &=\begin{bmatrix}1 & 0\\ -\mathbf{W} & 1\end{bmatrix}\begin{bmatrix}\mathbf{V}^{-1} & 0\\ 0 & (\mathbf{K}^t+\sigma^2\mathbf{I}_t)^{-1}\end{bmatrix}\\ &\quad\times\begin{bmatrix}1 & -\mathbf{U}\\ 0 & 1\end{bmatrix}.\end{aligned} \tag{41}$$

Besides, based on the joint PDF (35), the quadratic expansion of its exponential part can be expressed as (42), shown at the top of the next page. Thus, based on (36) and (42), it could be expressed as

$$p(f(\mathbf{x})|\mathbf{y}^t) = \mathcal{CN}\left(\mu(\mathbf{x})+\mathbf{U}(\mathbf{y}^t-\boldsymbol{\mu}^t),\mathbf{V}\right). \tag{43}$$

According to (43), the posterior mean (12), covariance (13) and variance (14) can be obtained and we complete the proof.

Appendix B
Proof of Lemma 2

First, we prove that

$$\Pr\left\{|\mathbf{g}(\boldsymbol{x})-\mu_{t-1}(\boldsymbol{x})| \le \sqrt{\beta_t}\sigma_{t-1}(\boldsymbol{x})\right\} \ge 1-\delta. \tag{44}$$

Specifically, we assume $\boldsymbol{g}_{t-1} = (g_1,\cdots,g_{t-1})$ and $\{\boldsymbol{x}_1,\cdots,\boldsymbol{x}_{t-1}\}$ are determined, and $\mathbf{g}(\boldsymbol{x}) \sim N(\mu_{t-1}(\boldsymbol{x}),\sigma^2_{t-1}(\boldsymbol{x}))$. Then, we set $r = \frac{\mathbf{g}(\boldsymbol{x})-\mu_{t-1}(\boldsymbol{x})}{\sigma_{t-1}(\boldsymbol{x})}$, $r \sim N(0,1)$ and $c = \beta_t$, we could get

$$\begin{aligned}\Pr\{r>c\} &= \frac{1}{\sqrt{2\pi}}\int_c^{\infty} e^{-\frac{r^2}{2}}dr\\ &= e^{\frac{-c^2}{2}}\frac{1}{\sqrt{2\pi}}\int_c^{\infty} e^{-\frac{(r-c)^2}{2}-c(r-c)}dr\\ &\le e^{\frac{-c^2}{2}}\Pr\{r>0\} = \frac{1}{2}e^{\frac{-c^2}{2}}.\end{aligned} \tag{45}$$

$$\begin{aligned}
&\left(\begin{bmatrix} f(\mathbf{x}) \\ \mathbf{y}^t \end{bmatrix} - \begin{bmatrix} \mu(\mathbf{x}) \\ \boldsymbol{\mu}^t \end{bmatrix}\right)^{\mathrm{T}} \begin{bmatrix} k(\mathbf{x},\mathbf{x}') & (\mathbf{k}^t(\mathbf{x}))^{\mathrm{H}} \\ \mathbf{k}^t(\mathbf{x}) & \mathbf{K}^t + \sigma^2\mathbf{I}_t \end{bmatrix}^{-1} \left(\begin{bmatrix} f(\mathbf{x}) \\ \mathbf{y}^t \end{bmatrix} - \begin{bmatrix} \mu(\mathbf{x}) \\ \boldsymbol{\mu}^t \end{bmatrix}\right) \\
&= \left(\begin{bmatrix} f(\mathbf{x}) \\ \mathbf{y}^t \end{bmatrix} - \begin{bmatrix} \mu(\mathbf{x}) \\ \boldsymbol{\mu}^t \end{bmatrix}\right)^{\mathrm{T}} \begin{bmatrix} 1 & 0 \\ -\mathbf{W}1 & \end{bmatrix} \begin{bmatrix} \mathbf{V}^{-1} & 0 \\ 0 & (\mathbf{K}^t + \sigma^2\mathbf{I}_t)^{-1} \end{bmatrix} \begin{bmatrix} 1-\mathbf{U} \\ 0 \ \ 1 \end{bmatrix} \left(\begin{bmatrix} f(\mathbf{x}) \\ \mathbf{y}^t \end{bmatrix} - \begin{bmatrix} \mu(\mathbf{x}) \\ \boldsymbol{\mu}^t \end{bmatrix}\right) \\
&= \begin{bmatrix} f(\mathbf{x}) - \mu(\mathbf{x}) - \mathbf{U}(\mathbf{y}^t - \boldsymbol{\mu}^t) \\ \mathbf{y}^t - \boldsymbol{\mu}^t \end{bmatrix}^{\mathrm{T}} \begin{bmatrix} \mathbf{V}^{-1} & 0 \\ 0 & (\mathbf{K}^t + \sigma^2\mathbf{I}_t)^{-1} \end{bmatrix} \begin{bmatrix} f(\mathbf{x}) - \mu(\mathbf{x}) - \mathbf{U}(\mathbf{y}^t - \boldsymbol{\mu}^t) \\ \mathbf{y}^t - \boldsymbol{\mu}^t \end{bmatrix} \\
&= (f(\mathbf{x}) - \mu(\mathbf{x}) - \mathbf{U}(\mathbf{y}^t - \boldsymbol{\mu}^t))^{\mathrm{T}}\mathbf{V}^{-1}(f(\mathbf{x}) - \mu(\mathbf{x}) - \mathbf{U}(\mathbf{y}^t - \boldsymbol{\mu}^t)) + (\mathbf{y}^t - \boldsymbol{\mu}^t)^{\mathrm{T}}(\mathbf{K}^t + \sigma^2\mathbf{I}_t)^{-1}(\mathbf{y}^t - \boldsymbol{\mu}^t) \qquad (42)
\end{aligned}$$

Therefore, by substituting r and c, we can obtain $\Pr\left\{|\mathbf{g}(\boldsymbol{x}) - \mu_{t-1}(\boldsymbol{x})| \geq \sqrt{\beta_t}\sigma_{t-1}(\boldsymbol{x})\right\} \leq e^{-\frac{\beta_t}{2}}$. According to the principle of applying union bound, then we can get $\Pr\left\{|\mathbf{g}(\boldsymbol{x}) - \mu_{t-1}(\boldsymbol{x})| \leq \sqrt{\beta_t}\sigma_{t-1}(\boldsymbol{x})\right\} \geq 1 - |\mathcal{W}|e^{-\frac{\beta_t}{2}}$. Let $|\mathcal{W}|e^{-\frac{\beta_t}{2}} = \frac{6\delta}{\pi^2 t^2}$, (44) holds as $\sum \frac{6}{\pi^2 t^2} = 1$.

Further, if $|\mathbf{g}(\boldsymbol{x}) - \mu_{t-1}(\boldsymbol{x})| \leq \sqrt{\beta_t}\sigma_{t-1}(\boldsymbol{x})$ holds, we can obtain

$$\begin{aligned}
r_t &= \mathbf{g}(\boldsymbol{x}^*) - \mathbf{g}(\boldsymbol{x}_t) \\
&\leq \mu_{t-1}(\boldsymbol{x}^*) + \sqrt{\beta_t}\sigma_{t-1}(\boldsymbol{x}^*) - \mathbf{g}(\boldsymbol{x}_t) \\
&\leq \mu_{t-1}(\boldsymbol{x}_t) + \sqrt{\beta_t}\sigma_{t-1}(\boldsymbol{x}_t) - \mathbf{g}(\boldsymbol{x}_t) \\
&\leq 2\sqrt{\beta_t}\sigma_{t-1}(\boldsymbol{x}_t). \qquad (46)
\end{aligned}$$

Based on (44) and (46), we can obtain

$$\Pr\left\{|r_t \leq 4\beta_t\sigma_{t-1}^2(\boldsymbol{x}_t)\right\} \geq 1 - \delta. \qquad (47)$$

As β_t is noncreasing, we can obtain that

$$\begin{aligned}
4\beta_t\sigma_{t-1}^2(\boldsymbol{x}_t) &\leq 4\beta_T\sigma^2(\sigma^{-2}\sigma_{t-1}^2(\boldsymbol{x}_t)) \\
&\overset{(a)}{\leq} 4\beta_T\sigma^2\frac{\sigma^{-2}}{\log(1+\sigma^{-2})}\log\left(1+\sigma^{-2}\sigma_{t-1}^2(\boldsymbol{x}_t)\right), \qquad (48)
\end{aligned}$$

where (a) holds since $\sigma^{-2}\sigma_{t-1}^2(\boldsymbol{x}_t) \leq \frac{\sigma^{-2}}{\log(1+\sigma^{-2})}\log\left(1+\sigma^{-2}\sigma_{t-1}^2(\boldsymbol{x}_t)\right)$ holds for $0 \leq \sigma^{-2}\sigma_{t-1}^2(\boldsymbol{x}_t) \leq \sigma^{-2}$.

Besides, for the information gain, we can derive that

$$I(\mathbf{g}_{\Omega_T};\mathbf{g}_T) = \frac{1}{2}\sum_{t=1}^{T}\log\left(1+\sigma^{-2}\sigma_{t-1}^2(\boldsymbol{x}_t)\right), \qquad (49)$$

for $I(\mathbf{g}_{\Omega_T};\mathbf{g}_T) = \mathrm{H}(\mathbf{g}_{\Omega_T}) - \frac{1}{2}\log|2\pi e\sigma^2\boldsymbol{I}|$ and $\mathrm{H}(\mathbf{g}_{\Omega_T}) = \mathrm{H}(\mathbf{g}_{\Omega_{T-1}}) + \mathrm{H}(\mathrm{g}_{\Omega_T}|\mathbf{g}_{\Omega_{T-1}}) = \mathrm{H}(\mathbf{g}_{\Omega_{T-1}}) + \frac{1}{2}\log(2\pi e(\sigma^2 + \sigma_{t-1}^2(\boldsymbol{x}_T)))$. Thus, by substituting (49) into (47) and (48), we can get

$$\Pr\left\{\sum_{t=1}^{T} r_t^2 \leq \frac{8\beta_T I(\mathbf{g}_{\Omega_T};\mathbf{g}_T)}{\log(1+\sigma^{-2})} \leq \frac{8\beta_T\gamma_T}{\log(1+\sigma^{-2})}\right\} \geq 1-\delta. \qquad (50)$$

Then, by applying the Cauchy-Schwarz inequality $R_T^2 \leq T\sum_{t=1}^{T} r_t^2$ into (50), we can get (33) and the proof is completed.

REFERENCES

[1] W. Saad, M. Bennis, and M. Chen, "A vision of 6G wireless systems: Applications, trends, technologies, and open research problems," *IEEE Netw.*, vol. 34, no. 3, pp. 134–142, Jun. 2019.

[2] Z. Wang et al., "A tutorial on extremely large-scale MIMO for 6G: Fundamentals, signal processing, and applications," *IEEE Commun. Surveys Tuts.*, vol. 26, no. 3, pp. 1560–1605, 3rd Quart., 2024.

[3] H. Lu et al., "A tutorial on near-field XL-MIMO communications toward 6G," *IEEE Commun. Surveys Tuts.*, vol. 26, no. 4, pp. 2213–2257, 4th Quart., 2024.

[4] M. Cui, Z. Wu, Y. Lu, X. Wei, and L. Dai, "Near-field MIMO communications for 6G: Fundamentals, challenges, potentials, and future directions," *IEEE Commun. Mag.*, vol. 61, no. 1, pp. 40–46, Jan. 2023.

[5] E. Björnson, Ö. T. Demir, and L. Sanguinetti, "A primer on near-field beamforming for arrays and reconfigurable intelligent surfaces," in *Proc. 55th Asilomar Conf. Signals Syst. Comput.*, Nov. 2021, pp. 105–112.

[6] K. T. Selvan and R. Janaswamy, "Fraunhofer and Fresnel distances: Unified derivation for aperture antennas," *IEEE Antennas Propag. Mag.*, vol. 59, no. 4, pp. 12–15, Aug. 2017.

[7] X. Gao, L. Dai, Z. Chen, Z. Wang, and Z. Zhang, "Near-optimal beam selection for beamspace mmWave massive MIMO systems," *IEEE Commun. Lett.*, vol. 20, no. 5, pp. 1054–1057, May 2016.

[8] M. Cui and L. Dai, "Channel estimation for extremely large-scale MIMO: Far-field or near-field?" *IEEE Trans. Commun.*, vol. 70, no. 4, pp. 2663–2677, Apr. 2022.

[9] H. Zhang et al., "Beam focusing for near-field multiuser MIMO communications," *IEEE Trans. Wireless Commun.*, vol. 21, no. 9, pp. 7476–7490, Sep. 2022.

[10] Y. Zhang, X. Wu, and C. You, "Fast near-field beam training for extremely large-scale array," *IEEE Wireless Commun. Lett.*, vol. 11, no. 12, pp. 2625–2629, Dec. 2022.

[11] X. Wu, C. You, J. Li, and Y. Zhang, "Near-field beam training: Joint angle and range estimation with DFT codebook," *IEEE Trans. Wireless Commun.*, vol. 23, no. 9, pp. 11890–11903, Sep. 2024.

[12] Y. Lu, Z. Zhang, and L. Dai, "Hierarchical beam training for extremely large-scale MIMO: From far-field to near-field," *IEEE Trans. Commun.*, vol. 72, no. 4, pp. 2247–2259, Apr. 2024.

[13] C. Wu, C. You, Y. Liu, L. Chen, and S. Shi, "Two-stage hierarchical beam training for near-field communications," *IEEE Trans. Veh. Technol.*, vol. 73, no. 2, pp. 2032–2044, Feb. 2024.

[14] X. Shi, J. Wang, Z. Sun, and J. Song, "Spatial-chirp codebook-based hierarchical beam training for extremely large-scale massive MIMO," *IEEE Trans. Wireless Commun.*, vol. 23, no. 4, pp. 2824–2838, Apr. 2024.

[15] Y. Xu et al., "Hashing beam training for near-field communications," 2024, *arXiv:2403.06074*.

[16] W. Liu et al., "Deep learning based beam training for extremely large-scale massive MIMO in near-field domain," *IEEE Commun. Lett.*, vol. 27, no. 1, pp. 170–174, Jan. 2023.

[17] X. Zhang, H. Zhang, C. Li, Y. Huang, and L. Yang, "Environment-specific beam training for extremely large-scale MIMO systems via contrastive learning," *IEEE Commun. Lett.*, vol. 27, no. 10, pp. 2638–2642, Oct. 2023.

[18] G. Jiang and C. Qi, "Near-field beam training based on deep learning for extremely large-scale MIMO," *IEEE Commun. Lett.*, vol. 27, no. 8, pp. 2063–2067, Aug. 2023.

[19] M. Zecchin, M. B. Mashhadi, M. Jankowski, D. Gunduz, M. Kountouris, and D. Gesbert, "LiDAR and position-aided mmWave beam selection with non-local CNNs and curriculum training," *IEEE Trans. Veh. Technol.*, vol. 71, no. 3, pp. 2979–2990, Mar. 2022.

[20] C. Weng, X. Guo, and Y. Wang, "Near-field beam training with hierarchical codebook: Two-stage learning-based approach," *IEEE Trans. Veh. Technol.*, vol. 73, no. 9, pp. 14003–14008, Sep. 2024.
[21] T. Zheng, J. Zhu, Q. Yu, Y. Yan, and L. Dai, "Coded beam training," *IEEE J. Sel. Areas Commun.*, vol. 43, no. 3, pp. 928–943, Mar. 2025.
[22] E. Brochu, V. M. Cora, and N. de Freitas, "A tutorial on Bayesian optimization of expensive cost functions, with application to active user modeling and hierarchical reinforcement learning," 2010, *arXiv:1012.2599*.
[23] C. K. I. Williams and C. E. Rasmussen, "Gaussian processes for regression," in *Proc. Adv. Neural Inf. Process. Syst.*, Nov. 1995, pp. 514–520.
[24] E. Schulz, M. Speekenbrink, and A. Krause, "A tutorial on Gaussian process regression: Modelling, exploring, and exploiting functions," *J. Math. Psychol.*, vol. 85, pp. 1–16, Aug. 2018.
[25] Z. Xiao, T. He, P. Xia, and X. Xia, "Hierarchical codebook design for beamforming training in millimeter-wave communication," *IEEE Trans. Wireless Commun.*, vol. 15, no. 5, pp. 3380–3392, May 2016.
[26] C. Han, L. Yan, and J. Yuan, "Hybrid beamforming for terahertz wireless communications: Challenges, architectures, and open problems," *IEEE Wireless Commun.*, vol. 28, no. 4, pp. 198–204, Aug. 2021.
[27] J. Sherman, "Properties of focused apertures in the Fresnel region," *IRE Trans. Antennas Propag.*, vol. 10, no. 4, pp. 399–408, Jul. 1962.
[28] J. Brady, N. Behdad, and A. M. Sayeed, "Beamspace MIMO for millimeter-wave communications: System architecture, modeling, analysis, and measurements," *IEEE Trans. Antennas Propag.*, vol. 61, no. 7, pp. 3814–3827, Jul. 2013.
[29] Z. Zhang, J. Zhu, L. Dai, and R. W. Heath Jr., "Successive Bayesian reconstructor for channel estimation in fluid antenna systems," *IEEE Trans. Wireless Commun.*, vol. 24, no. 3, pp. 1992–2006, Mar. 2025.
[30] S. Yang, B. Liu, Z. Hong, and Z. Zhang, "Bayesian optimization-based beam alignment for mmWave MIMO communication systems," in *Proc. IEEE 33rd Annu. Int. Symp. Pers., Indoor Mobile Radio Commun. (PIMRC)*, Sep. 2022, pp. 825–830.
[31] N. Srinivas, A. Krause, S. M. Kakade, and M. W. Seeger, "Information-theoretic regret bounds for Gaussian process optimization in the bandit setting," *IEEE Trans. Inf. Theory*, vol. 58, no. 5, pp. 3250–3265, May 2012.
[32] M. Cui, Z. Zhang, L. Dai, and K. Huang, "Ice-filling: Near-optimal channel estimation for dense array systems," 2024, *arXiv:2404.06806*.
[33] H. J. Kushner, "A new method of locating the maximum point of an arbitrary multipeak curve in the presence of noise," *J. Basic Eng.*, vol. 86, no. 1, pp. 97–106, 1964.
[34] A. Mockus, "On Bayesian methods for seeking the extremum," in *Proc. IFIP Tech. Conf.*, Jan. 1975, pp. 400–404.
[35] D. J. Lizotte, "Practical Bayesian optimization," Ph.D. dissertation, Dept. Comput. Sci., Univ. Alberta, Edmonton, AB, Canada, 2008.
[36] P. Auer, N. Cesa-Bianchi, and P. Fischer, "Finite-time analysis of the multiarmed bandit problem," *Mach. Learn.*, vol. 47, no. 2, pp. 235–256, 2002.
[37] Z. Xiao, H. Dong, L. Bai, P. Xia, and X.-G. Xia, "Enhanced channel estimation and codebook design for millimeter-wave communication," *IEEE Trans. Veh. Technol.*, vol. 67, no. 10, pp. 9393–9405, Oct. 2018.
[38] S. Lyu, Z. Wang, Z. Gao, H. He, and L. Hanzo, "Lattice-based mmWave hybrid beamforming," *IEEE Trans. Commun.*, vol. 69, no. 7, pp. 4907–4920, Jul. 2021.
[39] A. Alkhateeb, G. Leus, and R. W. Heath Jr., "Limited feedback hybrid precoding for multi-user millimeter wave systems," *IEEE Trans. Wireless Commun.*, vol. 14, no. 11, pp. 6481–6494, Nov. 2015.
[40] Q. Shi, M. Razaviyayn, Z.-Q. Luo, and C. He, "An iteratively weighted MMSE approach to distributed sum-utility maximization for a MIMO interfering broadcast channel," *IEEE Trans. Signal Process.*, vol. 59, no. 9, pp. 4331–4340, Sep. 2011.
[41] J. Zhu, Z. Wan, L. Dai, and T. Jun Cui, "Electromagnetic information theory-based statistical channel model for improved channel estimation," *IEEE Trans. Inf. Theory*, vol. 71, no. 3, pp. 1777–1793, Mar. 2025.
[42] X. Zhang, H. Zhang, and Y. C. Eldar, "Near-field sparse channel representation and estimation in 6G wireless communications," *IEEE Trans. Commun.*, vol. 72, no. 1, pp. 450–464, Jan. 2024.
[43] K. Chen, C. Qi, C.-X. Wang, and G. Y. Li, "Beam training and tracking for extremely large-scale MIMO communications," *IEEE Trans. Wireless Commun.*, vol. 23, no. 5, pp. 5048–5062, May 2024.
[44] W. Liu, C. Pan, H. Ren, F. Shu, S. Jin, and J. Wang, "Low-overhead beam training scheme for extremely large-scale RIS in near field," *IEEE Trans. Commun.*, vol. 71, no. 8, pp. 4924–4940, Aug. 2023.

Zhuo Xu (Graduate Student Member, IEEE) received the B.E. degree in communication engineering from Harbin Institute of Technology, Harbin, China, in 2023. He is currently pursuing the M.S. degree with the Department of Electronic Engineering, Tsinghua University, Beijing, China. His research interests include extremely large-scale MIMO (XL-MIMO), near-field MIMO communications, and AI for communications. He received the National Scholarship in 2020 and 2022.

Zijian Zhang (Graduate Student Member, IEEE) received the B.E. degree in electronic engineering from Tsinghua University, Beijing, China, in 2020, where he is currently pursuing the Ph.D. degree in electronic engineering.

He is an Amateur in wireless localization and robotics. He has authored several articles for IEEE JOURNAL ON SELECTED AREAS IN COMMUNICATIONS, IEEE TRANSACTIONS ON SIGNAL PROCESSING, IEEE TRANSACTIONS ON WIRELESS COMMUNICATIONS, and IEEE TRANSACTIONS ON COMMUNICATIONS. His research interests include massive MIMO, holographic MIMO (H-MIMO), reconfigurable intelligent surfaces (RISs), and fluid antenna systems (FASs). He received the National Scholarship in 2019 and 2024. In 2024, he won the Special Scholarship of Tsinghua University, which annually awards ten students out of over 40,000 graduate students at Tsinghua University. He was listed in Stanford University's World's Top 2% Scientists in 2023.

Linglong Dai (Fellow, IEEE) received the B.S. degree from Zhejiang University, Hangzhou, China, in 2003, the M.S. degree from China Academy of Telecommunications Technology, Beijing, China, in 2006, and the Ph.D. degree from Tsinghua University, Beijing, in 2011.

From 2011 to 2013, he was a Post-Doctoral Researcher with the Department of Electronic Engineering, Tsinghua University, where he was an Assistant Professor from 2013 to 2016, an Associate Professor from 2016 to 2022, and has been a Professor since 2022. He has co-authored the book *MmWave Massive MIMO: A Paradigm for 5G* (Academic Press, 2016). He has authored or co-authored over 100 IEEE journal articles and over 60 IEEE conference papers. He also holds over 20 granted patents. His current research interests include massive MIMO, reconfigurable intelligent surface (RIS), millimeter-wave and Terahertz communications, near-field communications, machine learning for wireless communications, and electromagnetic information theory. He has received five IEEE Best Paper Awards at IEEE ICC 2013, IEEE ICC 2014, IEEE ICC 2017, IEEE VTC 2017-Fall, IEEE ICC 2018, and IEEE GLOBECOM 2023. He has also received the Tsinghua University Outstanding Ph.D. Graduate Award in 2011, the Beijing Excellent Doctoral Dissertation Award in 2012, China National Excellent Doctoral Dissertation Nomination Award in 2013, the URSI Young Scientist Award in 2014, the IEEE Transactions on Broadcasting Best Paper Award in 2015, the Electronics Letters Best Paper Award in 2016, the National Natural Science Foundation of China for Outstanding Young Scholars in 2017, the IEEE ComSoc Asia–Pacific Outstanding Young Researcher Award in 2017, the IEEE ComSoc Asia–Pacific Outstanding Paper Award in 2018, China Communications Best Paper Award in 2019, the IEEE Access Best Multimedia Award in 2020, the IEEE Communications Society Leonard G. Abraham Prize in 2020, the IEEE ComSoc Stephen O. Rice Prize in 2022, the IEEE ICC Best Demo Award in 2022, and the National Science Foundation for Distinguished Young Scholars in 2023. He was listed as a Highly Cited Researcher by Clarivate Analytics from 2020 to 2023.